9 Particle Physics at DESY/HERA (H1)

K. Müller, P. Robmann, U. Straumann, and P. Truöl

in collaboration with:
C. Grab, Institut für Teilchenphysik der ETH, Zürich; S. Egli, M. Hildebrandt, and R. Horisberger, Paul–Scherrer–Institut, Villigen, and 39 institutes outside Switzerland

(H1 - Collaboration)

While now almost four years have passed since the H1-experiment at the electron-proton collider HERA at DESY in Hamburg has finished taking data, the analysis of these data continues. Eight papers have been published ([1]-[8]) and further results, some of them still preliminary, have been presented at the "XVIII. International Workshop on Deep-Inelastic Scattering and Related Subjects (DIS 2010)" in Florence [9] in April 2010 and at the "35$^{\text{th}}$ International Conference on High Energy Physics (ICHEP 2010)" in Paris [10] in July 2010, or will be communicated at the "XIX. International Workshop on Deep-Inelastic Scattering and Related Subjects (DIS 2011)" in Newport News, Virginia [11] in April 2011 ([12]-[28]).

The central aim of these analyses remains the exploration of proton structure and tests of quantum chromodynamics (QCD) predictions. This program entails e.g. the precise determination of the neutral and charged electroweak current cross sections at high momentum transfer leading to parton density functions (PDF) in pre-HERA inaccessible domains of Bjorken x and momentum transfer Q^2, now combining H1-data with those of the neighbouring ZEUS-collaboration, the precise measurement of the running coupling constant α_s through a variety of channels, diffractively produced final states, hidden and open charm and beauty production as well as a few remaining searches for states outside the Standard Model.

These topics have been addressed last year:

- Extension of the structure function measurements to high inelasticity and direct assessment of the longitudinal component using also data from the runs with lower energy proton beams [7] (see also last years annual report for details [29]).

- Using neutral and charged current data with polarized beams for a combined electroweak and QCD fit [15], combining H1 and ZEUS structure function data for improved next-to-next-to-leading order (NNLO) PDF fits (HERAPDF1.5 NNLO) [12; 13], extending the combination procedure to the charm contribution $F_2^{c\bar{c}}$ [14].

- Search for contact interactions [28], squarks [6], and lepton flavor violation [8].

- Improved determination of the strong coupling α_s through combination of the H1 and ZEUS inclusive and jet production cross sections [16], as well as through a refined analysis of H1 data on multijet production at high Q^2 [17].

- Various aspects of charm and beauty production through D^*-tagging (see below for details) or lifetime-tagging [4; 25–27].

- Analysis of different exclusive channels [2; 18; 23; 24], e.g. by using the very forward proton and neutron spectrometers [1; 5; 19], as well as the isolation of the diffractive contributions to different channels [3; 20–22].

With the advent of the LHC graduate students from the Swiss institutions no longer contribute to the analyses. We continue, however, to serve as referees in the diffraction (Katharina Müller) and the heavy flavour (Christoh Grab and Peter Truöl) working groups.

9.1 D^* tagged photo- and electroproduction of charm

Charm and beauty production have been addressed by both HERA collaborations since 1996 with increasing statistics and detail. These measurements have confirmed the notion that heavy quarks are predominantly produced via boson-gluon fusion, $\gamma g \to c\bar{c}$ or ÃŁ$\gamma g \to b\bar{b}$, which is sensitive to the gluon density in the proton and allows its universality to be tested. The photon is radiated from the incoming lepton and the gluon from the proton. The cross section is largest for photoproduction, i.e. for photons with virtuality $Q^2 \approx 0$ GeV^2, but the production of charm quarks contributes up to 20 % to the inclusive ep scattering cross section for higher momentum transfer. Therefore, the correct treatment of the effects related to the charm quark contribution, in particular the mass effects, in perturbative QCD calculations is important for the determination of parton distribution functions, where different schemes to incorporate these effects are available. In addition to the case where the photon enters the hard process directly, one has also to consider the case where the partonic structure of the photon is resolved.

One of the pioneering articles in this area was based on the theses of two UZH graduate students, David Müller and Martin zur Nedden. It presented the first analysis where photo- and electroproduction of charmed quarks was directly linked to the gluon density [30]. $D^{*\pm}$ based charm tagging was applied, too, as in part of the later work [31; 32]. This technique makes use of the fact, that the decay chain:

$$D^{*\pm}(2010) \to D^0(1865)\pi^{\pm}_{\rm slow} \to K^{\mp}\pi^{\pm}\pi^{\pm}_{\rm slow}$$

distinguishes itself by a clear peak at 145 MeV in the distribution of the invariant mass difference ΔM:

$$\Delta M = M(K^{\mp}\pi^{\pm}\pi^{\pm}_{\rm slow}) - M(K^{\mp}\pi^{\pm})$$

This is demonstrated in Figs. 9.1 and 9.2, which compare the early results [30] with those from the most recent analyses to be discussed here [33; 34].

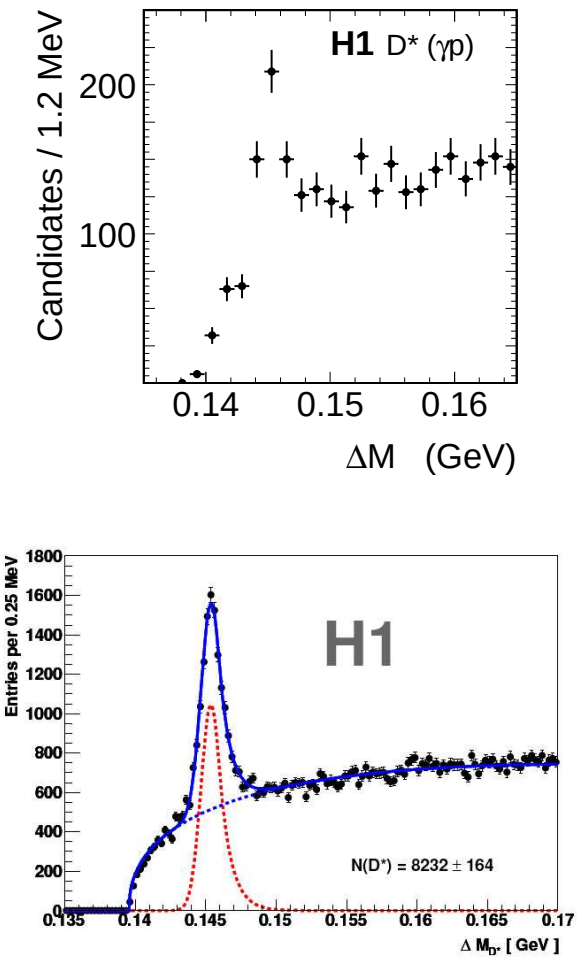

Fig. 9.1 – Distribution of ΔM for D^* candidates in photoproduction. Top: first H1-data from 1999 [30] (489±92 events, 60 % of total sample). Bottom: new data including the fit function [33].

The latter are based on an integrated luminosity of 93 and 348 pb^{-1}, for photoproduction and deep-inelastic scattering (DIS), respectively, compared to 10 and 21 pb^{-1} in the old analysis, with apparent improvement in the number of events observed. The momenta of the charged decay products were measured in the central tracking detectors. In the DIS case the events were triggered by an electromagnetic cluster in the backward electromagnetic calorimeter SPACAL. In the photoproduction case the new data had to rely on the fast-track-trigger (FTT) based on information from the central jet chamber, while in the old data photo-

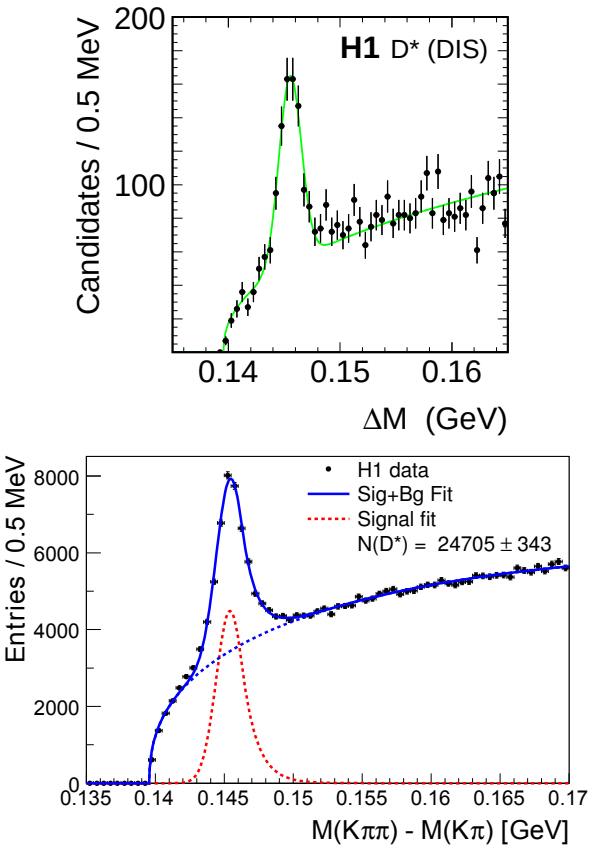

Fig. 9.2 – Distribution of ΔM for D^* candidates in deep inelastic scattering. Top: first H1-data from 1999 [30] (583±35 events). Bottom: new data including the fit function [34].

produced events could be triggered by signals in the low scattering angle electron taggers at 33 and 44 m downstream of the electron beam (ETAG33 and ETAG44). Skipping details of the analyses, of the normalisation procedures and of the evaluation of the systematic errors, selected results are displayed in Figs. 9.3 – 9.6.

Figure 9.3 shows the differential cross section for photoproduction as function of the invariant mass of the photon-proton system and of the transverse momentum p_T of the D^*. The data are compared to two theoretical calculations. In one of them, labeled FMNR [35] the production of heavy quarks is calculated in the so called massive scheme, where heavy quarks are produced only perturbatively via boson gluon fusion. In the alternative massless scheme the heavy quarks are treated as massless partons. These two schemes should be appropriate in different regions of phase space, the massive scheme should be reliable when the transverse momentum p_T of the heavy quarks is of similar size compared to the charm mass m_c ($\approx$ 1.5 GeV) , whereas the massless scheme is expected to be valid for $p_T > m_c$. Calculations in the general-mass variable-flavour-number scheme (GMVFNS) [36] combine the massless with the massive scheme. In the FMNR program a NLO calculation in the collinear approach is implemented, i.e. transverse momenta are generated in the hard scattering process and effects from the finite transverse momenta of the gluons enter only at NLO. The resolved and direct processes are calculated separately providing weighted parton level events with two or three outgoing partons, i.e. a charm quark pair and pos-

Fig. 9.3 – Differential D^* cross section as a function of the invariant mass of photon-proton system $W_{\gamma p}$ and of the D^* transverse momentum $p_T(D^*)$ compared to the next-to-leading order calculations FMNR [35] and GMVFNS [36]. The normalized ratio theory/experiment $R^{\rm norm}$ is also shown, which allows comparison of the shape independent of the normalisation.

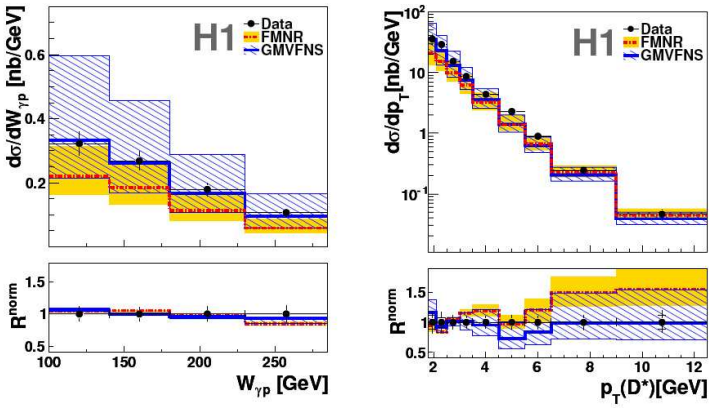

sibly one additional light parton. In the adaptation to the HERA data both calculations use the HERAPDF1.0-set for the proton [38] but slightly different PDF's for the photon and also slightly

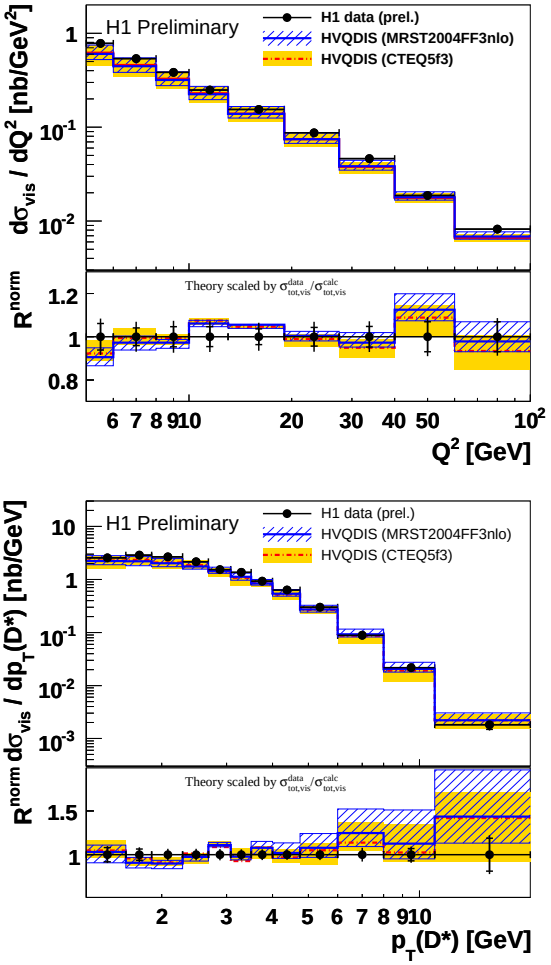

Fig. 9.4 – Differential D^* cross section as a function of the photon virtuality Q^2 (top) and the transverse momentum $p_T(D^*)$ (bottom) in the visible kinematical range of $5 < Q^2 < 100$ GeV^2, inelasticity $0.02 < y < 0.7$, pseudorapidity $|\eta(D^*)| < 1.8$ and $p_T(D^*) > 1.25$ GeV/c. The inner error bars show the statistical error, the outer error bars include the systematic errors. The measured data are compared to predictions by the next-to-leading order calculation HVQDIS [37] with two different proton parton densities. The bands indicate the theoretical uncertainties.

different fragmentation functions for the charmed quarks. The influence of these choices as well that of m_c and of the renormalisation and factorisation scales is reflected in the uncertainty bands of the models. The precision of the measurements is much higher than the accuracy of the NLO calculations. The uncertainty of the NLO predictions is dominated by the variation of the renormalisation scale, which leads to a large change in the normalisation, but only small differences in the shapes of some distributions. Within these large uncertainties, both NLO predictions agree with the cross section as a function of $p_T(D^*)$ and $W_{\gamma p}$.

A selection of the deep inelastic scattering data is shown in Figs. 9.4 – 9.6. The dependence of the cross section on Q^2 and $p_T(D^*)$ is again compared to a fixed order NLO calculation (HVQDIS) [37] based on collinear factorisation and the DGLAP evolution equations. This calculation assumes three active flavours (u, d, s) in the proton (fixed-flavour number scheme: FFNS) and massive charm quarks are produced dynamically, predominantly via boson gluon fusion. The total visible cross section has been measured to be $\sigma_{\mathrm{vis,tot}}(e^{\pm}p \to e^{\pm}D^{*\pm}X) = 6.44 \pm 0.09\,(\mathrm{stat.}) \pm 0.49\,(\mathrm{syst.})$ nb, while HVQDIS predicts typically 5.7 ± 1.3 nb. The visible region is defined in Fig. 9.4. For the comparison to an alternative NLO calculation based on the zero-mass variable flavour-number scheme (ZM-VFNS) [39], where the charm quark is considered as a massless constituent of the proton we must refer to the H1-publication [34]. Within the uncertainties introduced by the choice of the model parameters HVQDIS seems to describe the data well, while ZM-VFNS is less successful.

The charm contribution $F_2^{c\bar{c}}(x, Q^2)$ to the proton structure function is obtained via the expression for the one photon exchange cross section for charm production

$$\frac{d^2\sigma^{c\bar{c}}}{dxdQ^2} = \frac{2\pi\alpha_{em}^2}{Q^4 x} \times \left(\left[1 + (1-y)^2\right] F_2^{c\bar{c}}(x, Q^2) - y^2 F_L^{c\bar{c}}(x, Q^2)\right),$$

where α_{em} is the electromagnetic coupling constant. The contribution from $F_L^{c\bar{c}}$ is small in the present phase space. The visible inclusive $D^{*\pm}$ cross sections in bins of inelasticity y and

Q^2 can be converted to a bin centre corrected $F_2^{c\bar{c}\,exp}(\langle x\rangle, \langle Q^2\rangle)$ by extrapolating the visible cross sections to the full phase space using input from HVQDIS. The small beauty contribution is subtracted, too. The uncertainty of this extrapolation procedure is included in the systematic error [34].

Figures 9.5 and 9.6 show results for $F_2^{c\bar{c}}$. They agree very well with the independent H1-measurement using the lifetime charm tag obtained from the central silicon vertex detector CST built by the Swiss groups [40]. The FFNS NLO calculation gives a good description of the data with either choice of two recently published proton PDFs (see [34] for references). Equally well does HERAPDF1.0, which has been extracted from the combined inclusive proton structure function data of the H1 and ZEUS detectors in a general-mass variable-flavour-number scheme, interpolating between FFNS and the ZM-VFNS [38].

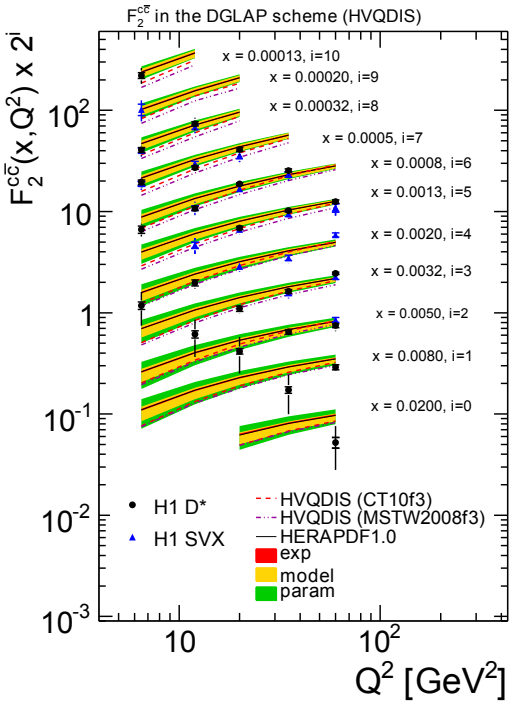

Fig. 9.5 – $F_2^{c\bar{c}}$ as a function of Q^2 for different x, as derived in the framework of NLO DGLAP. The inner error bars show the statistical, the outer error bar the total uncertainty which includes statistical, experimental systematic, extrapolation and model uncertainty added in quadrature. Also shown are the results using the H1 vertex detector (H1 SVX) [40], NLO DGLAP predictions from HVQDIS [37] with two different proton PDFs, and HERAPDF1.0 predictions [38].

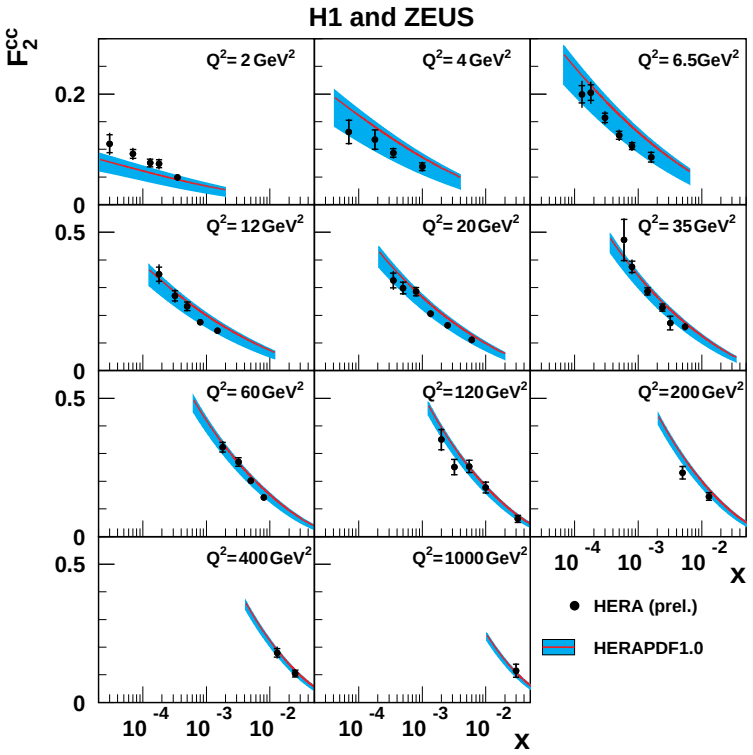

Fig. 9.6 – Combined results for $F_2^{c\bar{c}}$ from H1 and ZEUS using different charm tagging methods. Uncertainties of 5-10 % are achieved in the explored region $2 < Q^2 < 1000$ GeV^2 and $10^{-5} < x < 10^{-1}$ [14]. The spread in the HERAPDF1.0 prediction reflects the uncertainty in the charm quark mass 1.354$< m_c <$1.65 GeV.

The uncertainty on $F_2^{c\bar{c}}$ for the HERAPDF1.0 prediction is dominated by the variation of the charm mass in the PDF fit. The agreement attests to the fact that the gluon density determined from the scaling violations of the inclusive proton structure function is consistent with the one needed in charm production. A recent analysis of the combined $F_2^{c\bar{c}}$ data from H1 and ZEUS [14] has demonstrated that the inclusion of the charm data can restrict the allowed range of m_c considerably. This then has consequences for the accuracy of the predictions for e.g. W-boson production at LHC energies.

[1] F.D. Aaron *et al.* [H1], Eur. Phys. J. C **68** (2010) 381.

[2] F.D. Aaron *et al.* [H1], Eur. Phys. J. C **68** (2010) 401.

[3] F.D. Aaron *et al.* [H1], Eur. Phys. J. C **70** (2010) 15.

[4] F.D. Aaron *et al.* [H1], Eur. Phys. J. C **71** (2011) 1509.

[5] F.D. Aaron *et al.* [H1], Eur. Phys. J. C **71** (2011) 1578.

[6] F.D. Aaron *et al.* [H1], Eur. Phys. J. C **71** (2011) 1572.

[7] F.D. Aaron *et al.* [H1], Eur. Phys. J. C (2011), in print.

[8] F.D. Aaron *et al.* [H1], Phys. Lett. B (2011), in print.

[9] Contributions to XVIII. International Workshop on Deep-Inelastic Scattering and Related Subjects (DIS 2010), Florence, Italy, April 19-23, 2011[5].

[10] Contributions to 35th International Conference on High Energy Physics, Paris, France, July 21-28, 2010 [5].

[11] Contributions to XIX. International Workshop on Deep-Inelastic Scattering and Related Subjects (DIS 2011), Newport News, April 11-16, 2011[5].

[12] *H1 and ZEUS combined measurement of neutral and charged current cross sections at HERA* [10]

[13] *H1 + ZEUS pdf fits including HERA-II high Q^2 data (HERAPDF1.5 NNLO)* [10; 11]

[14] *QCD analysis of combined H1 and ZEUS $F_2^{c\bar{c}}$ data* [11]

[15] *Combined electroweak and QCD fit of inclusive neutral and charged current data with polarized lepton beams at HERA* [11]

[16] *QCD analysis with determination of α_s based on HERA inclusive and jet data (H1+ZEUS)* [11]

[17] *Measurement of multijet production and α_s in deep-inelastic ep-scattering at high Q^2* [11]

[18] *Measurement of the azimuthal correlation between the scattered electron and the most forward jet in deep-inelastic scattering at HERA* [10; 11]

[19] *Very forward photon spectrum and neutron P_T distribution measured with the forward neutron calorimeter (FNC)* [10; 11]

[20] *Measurement of the diffractive structure function F_2^{D3} with the very forward proton spectrometer (VFPS)* [9]

[21] *Exclusive diffractive J/ψ production at low $W_{\gamma p}$* [11]

[22] *Dijet production in diffractive deep inelastic scattering using the very forward proton spectrometer (VFPS)* [11]

[23] *Transverse momentum of charged particles in an extended pseudorapidity range* [9; 11]

[24] *K_s^0 production at high Q^2 at HERA II* [9]

[25] *D^* production at low Q^2 in an extended phase space* [10]

[26] *D^* with jets in photoproduction* [9]

[27] *Measurement of the photoproduction of b-quarks at threshold at HERA* [11]

[28] *Search for contact interactions at HERA* [10]

[5] www-h1.desy.de/publications/H1preliminary.short.list.html

[29] Physik-Institut, University of Zürich, Annual Reports 1996/7 ff.; available at *http://www.physik.uzh.ch/reports.html*

[30] C. Adloff *et al.* [H1], Nucl. Phys. B **545** (1999) 21.

[31] A. Aktas *et al.* [H1], Eur. Phys. J. C **50** (2007) 251.

[32] F. D. Aaron *et al.* [H1], Phys. Lett. B **686** (2010) 91; A. Aktas *et al.* [H1], Eur. Phys. J. C **51** (2007) 271; C. Adloff *et al.* [H1], Phys. Lett. B **528** (2002) 199; C. Adloff *et al.* [H1], Z. Phys. C **72** (1996) 593.

[33] *Measurement of inclusive D^* meson cross sections in photoproduction at HERA*[5].

[34] *Measurement of inclusive $D^{\pm}$ meson production and determination of $F_2^{c\bar{c}}$ at low Q^2 in deep-inelastic scattering at HERA*, F.D. Aaron *et al.* [H1], submitted to Eur. J. Phys. C; see also [25].

[35] S. Frixione *et al.*, Phys. Lett. B **308** (1993) 137; S. Frixione, P. Nason and G. Ridolfi, Nucl. Phys. B **454** (1995) 3.

[36] G. Kramer and H. Spiesberger, Eur. Phys. J. C **38** (2004) 309; B. A. Kniehl *et al.*, Eur. Phys. J. C **62** (2009) 365.

[37] B.W. Harris and J. Smith, Phys. Rev. D **57** (1998) 2806; idem Nucl. Phys. B **452** (1995) 109.

[38] F.D. Aaron *et al.* [H1/ZEUS], JHEP **1001** (2010) 109.

[39] G. Heinrich and B. A. Kniehl, Phys. Rev. D **70** (2004) 094035; C. Sandoval, *Inclusive production of hadrons in neutral and charged current ceep inelastic scattering*, DESY-THESIS-2009-044, Ph.D. Thesis Univ. Hamburg (2009).

[40] F. D. Aaron *et al.* [H1], Eur. Phys. J. C **65** (2010) 89.